

## Films of Heusler alloys

J. DUBOWIK<sup>1\*</sup>, I. GOŚCIAŃSKA<sup>2</sup>, A. SZLAFEREK<sup>1</sup>, Y. V. KUDRYAVTSEV<sup>3</sup>

<sup>1</sup>Institute of Molecular Physic, Polish Academy of Sciences, Poznań 60-179, Poland

<sup>2</sup>Department of Physics, Adam Mickiewicz University, Poznań 61-614, Poland

<sup>3</sup>Institute of Metal Physics, National Academy of Sciences of Ukraine, 252680 Kiev-142, Ukraine

Heusler alloys (HA) are a class of materials which may be metals, semiconductors or semimetals, most of them being ferromagnets. Some new applications of HA in spintronics and micro-electromagnetic actuators require their preparation in the form of thin films. Deposition of a HA film is a challenging task from the point of view of its proper ordering. Local disorder and antisite disorder are the most probable reasons of failure in achieving 100% polarization in nanostructures containing HA layers. We will review some examples of tunnel magnetoresistance structures that include Co<sub>2</sub>YZ HA layers (Y = Mn, Cr, Fe, Z = Al, Si, Ga). The influence of structural ordering on the magnetic and transport properties of Co<sub>2</sub>MnGa films are given with an emphasis on crystallization process of the films with amorphous structure and a further improvement of its structural ordering. Equally difficult task concerns preparation of HA films with shape memory (SM) effect. Recent achievements in technology of HA with SM will be reviewed. We will focus on non-stoichiometric Ni–Mn–Ga sputtered films. Their SM properties critically depend on composition and post-deposition annealing conditions. By a proper choice of these conditions, the ordered Ni–Mn–Ga films exhibit a well defined SM effect near room temperature.

Key words: *Heusler alloy; thin film; half-metal; ferromagnetic shape memory*

### 1. Introduction

Heusler alloys (HA) with the chemical formula X<sub>2</sub>YZ are a class of materials with a variety of interesting physical properties. Depending on composition, they may be metals, semiconductors or semimetals, and additionally, most of them are ferromagnets. The full Heusler structure consists of four interpenetrating *fcc* sublattices with atoms at A(0,0,0), C(1/2,1/2,1/2), B(1/4,1/4,1/4), and D(3/4,3/4,3/4) positions which results in *L*<sub>21</sub> crystal structure of the so-called full HA (Fig. 1) in which X<sub>1</sub> and X<sub>2</sub> sublattices are fully occupied. A large number of different elements can be chosen for

---

\*Corresponding author, e-mail: dubowik@ifmpan.poznan.pl

X (Ni, Co, Fe, Pd, ...), Y (Mn, Ni, Fe, Co, Ti, ...), and Z (Ga, Al, In, Si, ...) offering rich possibilities for tuning their magnetic, electrical and mechanical properties.

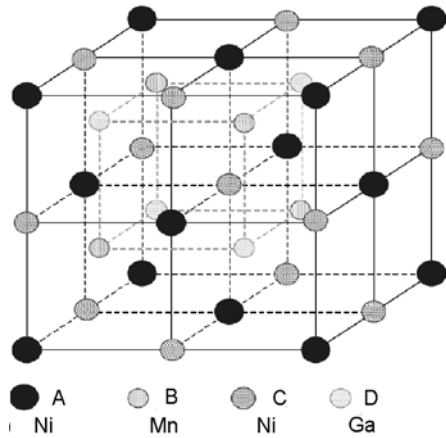


Fig. 1. Crystal structure of  $X_2YZ$  full Heusler alloy displaying the  $L2_1$  structure consisting of four interpenetrating fcc lattices (A, B, C, D), each occupied by one of the following elements: Ni, Mn, or Ga

In HA there is always some degree of chemical disorder, heavily influencing many of their physical properties. In the fully ordered HA, the four sublattices A, B, C, and D are occupied by X, Y, X, and Z atoms, respectively giving the  $L2_1$  type of order as it is shown in Fig. 1. In reality, this fully ordered state is hard to be attained, and there is a variety of possible disorder [1]. When X atoms remain ordered and full disorder occurs between Y and Z sites only, we have a  $B2$  (CsCl type) structure, for example. If disorder occurs between one X site and either Y or Z sites, the atomic arrangement may lead to a  $DO_3$  ( $Fe_3Al$ ) structure. And eventually, an  $A2$  structure occurs if there is the atomic arrangement when random order occurs between all X, Y and Z sites.

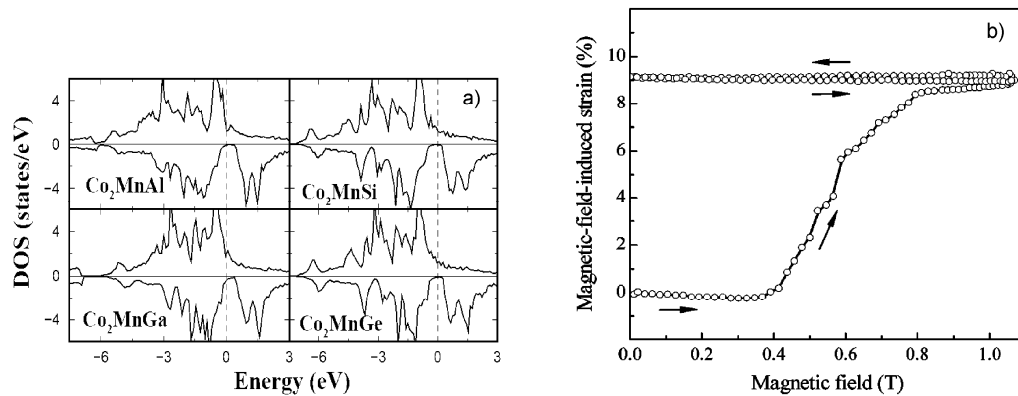


Fig. 2. Spin-resolved DOS for  $Co_2MnX$ , X = Al, Si, Ga, Ge (from Ref. [2]) (a) with a spin-split band structure characteristic of insulating behaviour of the spin down electrons; field-induced strain of a single-variant sample of orthorhombic seven-layered phase in the  $Ni_{48.8}Mn_{29.7}Ga_{21.5}$  alloy at 300 K (b) measured perpendicular to the magnetic field applied along the (100) direction (from Ref. [7])

Recently, HA has attracted attention since they show great potential for spintronic [2] or for electromechanical [3, 4] applications. The first aspect concerns half-metallic properties of some HA exhibiting 100% spin polarization at the Fermi level. Full spin polarization results from two types of band structures for the majority and minority spin bands: while the majority spin band shows a typical metallic behaviour, the minority spin band exhibits a semiconducting behaviour with a gap in density of states at the Fermi level (Fig. 2a). NiMnSb half Heusler compound was found to reveal a half metallic behaviour as early as in 1983 [5], but full HA such as Co<sub>2</sub>MnSi or Co<sub>2</sub>MnGe [6] have only recently been found (by electron energy band calculations) to possess full spin polarization.

The second aspect is related to shape memory effect of some HA – a reversible martensitic transformation resulting in a substantial mechanical strain. Ni<sub>2</sub>MnGa is the best known HA which exhibits both ferromagnetic behaviour and structural instabilities leading to a low temperature tetragonal distortion of the cubic cell, i.e., a martensitic transformation [3]. Additionally, for off-stoichiometric Ni–Mn–Ga HA, the martensitic transformation temperature may be tuned close to room temperature and various kinds of modulated structures in the martensitic phase may occur. It appeared that in such structurally metastable martensite phase, a rearrangement of martensitic variants can be realized under application of a relatively low magnetic field. As is shown in Fig. 2b, application of the magnetic field of ~1 T results in a huge (~10%) strain [7]. This effect is known as ferromagnetic shape memory effect (FSM). Recently a similar field-induced FSM effect has been found in non-stoichiometric Ni<sub>50</sub>Mn<sub>25+x</sub>Sn<sub>25-x</sub> HA [8].

It is obvious that for any spintronic application one needs HA in the form of thin films. Therefore, a number of papers have been concerned with both theoretical aspects of half-metallic behaviour of the HA thin films as well as with technological aspects aimed at fabrication of HA films with the highest spin polarization under optimum conditions (see, for example Ref. [2]). The formation of a HA film is a challenging task from the point of view of a proper ordering of different elements into the four sublattices. Local disorder and antisite disorder effects are the most probable reasons of failure in achieving 100% polarization in nanostructures containing HA layers.

Equally difficult task concerns preparation of HA films exhibiting ferromagnetic shape memory effect. Single crystals of off-stoichiometric Ni–Mn–Ga alloy exhibit strains of 10% under application of a moderate magnetic field [7] but in the films the effect has been found to be much lower [9]. Recent achievements in the thin film technology of FSM alloys comprise thin Ni–Mn–Ga films deposited by molecular beam epitaxy (MBE) [10], laser ablation [11] and by sputtering [12]. Since their shape memory properties critically depend on composition and post-deposition annealing conditions, and by a constraint from a substrate, by a proper choice of the deposition conditions and post-deposition annealing, the ordered and partially or fully released Ni–Mn–Ga films exhibit a well defined shape memory effect near room temperature.

## 2. Electronic transport in Heusler alloy films

Spintronics, which uses the spin degrees of freedom, is currently attracting great interest due to a high potential for applications in magnetic sensors and other devices based on tunnel magnetoresistive effect [13]. Hence, the materials with a high degree of spin polarization  $P$  at the Fermi level are needed to ensure as high as possible tunnel magnetoresistance ratio (TMR):

$$\text{TMR} = \frac{R_{\uparrow\downarrow} - R_{\uparrow\uparrow}}{R_{\uparrow\uparrow}} = \frac{2P_1P_2}{1 - P_1P_2} \quad (1)$$

where  $R_{\uparrow\downarrow}$  and  $R_{\uparrow\uparrow}$  are resistances for antiparallel and parallel magnetization configurations in a magnetic tunnel junction (MTJ), respectively. This definition gives  $\text{TMR} = \infty$  (in practice a very high value of  $\sim 10^4$ ) for the full polarization  $P_1 = P_2 = 100\%$  of the two ferromagnetic electrodes in TMJ.

A systematic search (based on electronic band calculations) for HA has revealed that  $\text{Co}_2\text{MnGe}$ ,  $\text{Co}_2\text{MnAl}$ ,  $\text{Co}_2\text{MnSi}$  and  $\text{Co}_2\text{MnGa}$  may be regarded as half-metallic ferromagnets with full (or almost full) spin polarization at the Fermi level [2, 6]. Recently, a considerable effort was devoted to HA containing Cr– $\text{Co}_2\text{CrAl}$  and  $\text{Co}_2\text{Cr}_{1-x}\text{Fe}_x\text{Al}$  – since they have been also predicted to exhibit a complete spin polarization with both a high magnetization and a high Curie temperature [14, 15].  $\text{Co}_2\text{Cr}_{1-x}\text{Fe}_x\text{Al}$  HA showed a high magnetoresistive effect of 60% in pressed powder pallets [14] and since this discovery a number of theoretical papers has confirmed their full polarization [16, 17]. However, in a spin valve MTJ containing  $\text{Co}_2\text{Cr}_{0.6}\text{Fe}_{0.4}\text{Al}$  electrode only a moderate TMR of  $\sim 16\%$  has been found at RT [18].

Despite the predicted half-metallic properties of HA, in HA films much less than 100% spin polarization has been measured so far (see, for example, Ref. [19]). There are few useful methods of determining spin polarizations in ferromagnetic materials. Photoemission [20] and tunnelling spectroscopy [21] have been applied but the most appropriate seems to be point-contact Andreev reflection [22] in which a measurement of the conductance between a superconductor in a point contact with a ferromagnet can determine the spin polarization. Using this method, Clifford et al. [23] found the spin polarization of  $\sim 80\%$  in  $\text{Co}_2\text{Cr}_{0.6}\text{Fe}_{0.4}\text{Al}$  bulk HA. The most extensively applied method, however, for the measurement of the spin polarization in half-metallic thin films is evaluation of  $P$  from TMR effect in MTJ devices. Using a CoFe layer ( $P \approx 50\%$ ) as a top electrode and a HA film as a bottom electrode [24] the resulting spin polarization can be simply estimated from the Juliere model described by Eq. (1). Keeping in mind that the magnetoresistance of such an MTJ depends not only on the electronic structure of HA but also on the quality of insulating barrier ( $\text{AlO}_x$  in most cases), one may regard the resulting spin polarization of HA as a realistic limit determined both by a structural perfection of HA film and a HA/tunnel barrier interface quality on equal foot. On the other hand, such an approach gives some practical

insight on the realization of HA electrodes integrated with other components of an MTJ device.

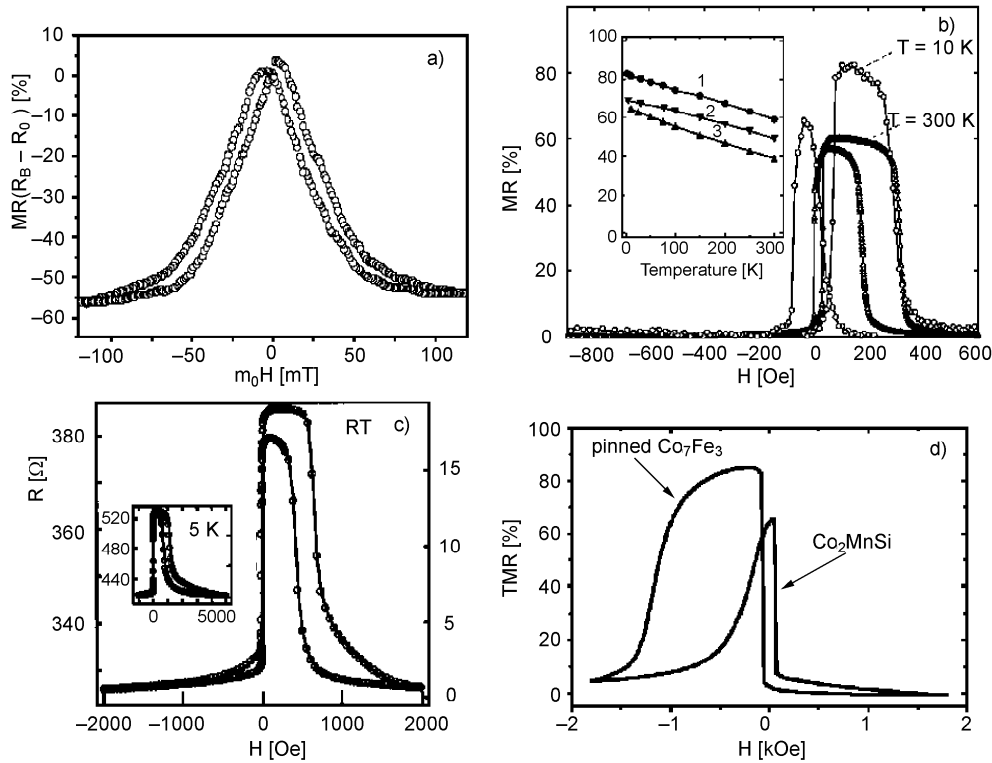


Fig. 3. Magnetoresistance (MR) of a powder pellet of  $\text{Co}_2\text{Cr}_{0.6}\text{Fe}_{0.4}\text{Al}$  (from Ref. [14]) (a); MR curves of MTJ with the epitaxial  $\text{Co}_2\text{MnAl}$  bottom electrode at 10 K and 300 K (b); the inset shows temperature dependence of MR ratios for MTJ using epitaxial  $\text{Co}_2\text{MnAl}$  (1), polycrystalline  $\text{Co}_2\text{MnAl}$  (2), and  $\text{Co}_{75}\text{Fe}_{25}$  (3) (from Ref. [26]); magnetoresistance curves at RT and 5 K for a spin-valve-type MTJ with a  $\text{Co}_2\text{Cr}_{1-x}\text{Fe}_x\text{Al}$  electrode (from Ref. [21]) (c); MR loop of MTJ (d) with  $\text{Co}_2\text{MnSi}$  Heusler alloy electrode (from Ref. [28])

Figure 3 juxtaposes some recent results concerning TMR characteristics of MTJ devices which include a HA layer as a bottom electrode. However, the most puzzling result (shown in Fig. 3a) concerns a relatively high TMR effect of  $\sim 60\%$  at RT in pressed powder pellets of  $\text{Co}_2\text{Cr}_{0.6}\text{Fe}_{0.4}\text{Al}/\text{Al}_2\text{O}_3$  [14]. Such a high value of TMR in the obviously defected samples with nonuniform microstructure resulted in further attempts [18, 25] aimed at fabrication of MTJ containing  $\text{Co}_2\text{CrFeAl}$  HA electrode with structural ordering as good as possible. However, as is seen in Fig. 3b, TMR in a spin valve structure  $\text{Co}_2\text{Cr}_{1-x}\text{Fe}_x\text{Al}$  (100 nm)/ $\text{Al}_2\text{O}_3$ (1.3 nm)/ $\text{CoFe}$ (3 nm)/ $\text{NiFe}$  (5nm)/ $\text{IrMn}$  (15 nm)/ $\text{Ta}$  (10 nm) has been found fairly low amounting to  $\sim 19\%$  at RT for  $x = 0.4$  [25]. It appeared that HA films prepared by magnetron sputtering on thermally oxidized Si substrates do not show the  $L2_1$  structure as expected for the bulk, but reveal the  $B2$  or

$A2$  structures, depending on Fe concentration. It was pointed out that better TMR characteristics might be obtained for  $B2$  structure without Co–Cr type of disorder.

Recently Sakubara et al. [26] fabricated MTJ with epitaxially grown  $\text{Co}_2\text{MnAl}$  bottom electrodes combined with a magnetron sputtered Al–O tunnel barrier. As shown in Fig. 3c, MTJ with a stacking structure of epi- $\text{Co}_2\text{MnAl}/\text{AlO}/\text{CoFe}/\text{IrMn}$  exhibits  $\text{TMR} \approx 65\%$  at RT and  $83\%$  at 2 K (see the inset in Fig. 3c). This result suggested that  $\text{Co}_2\text{MnAl}$  with  $B2$  order is highly spin polarized, however the estimated spin-polarization of  $\sim 59\%$  (Eq. (1)) is still smaller than the expected value of  $76\%$  for the  $B2$  structure [27]. Besides TMJ containing  $\text{Co}_2\text{Cr}_{1-x}\text{Fe}_x\text{Al}$  or  $\text{Co}_2\text{MnAl}$  HA electrodes,  $\text{Co}_2\text{MnSi}$  HA integrated in MTJ [28] offers even higher TMR values of  $\sim 86\%$  at 10 K which roughly corresponds to  $P = 60\%$  (Fig. 3d). Recently, Hütten et al. [24] demonstrated TMR value of  $108\%$  at 20 K associated with the spin polarization of  $72\%$ . All these results clearly show that fabrication of MTJ or other spintronic devices in which HA electrodes would reveal full half-metallic characteristics (i.e.  $\text{TMR} \approx \infty$ ) is still a challenging task, first of all, due to difficulties in preparation of HA layers with a good ordering, and secondly, due to difficulties with oxidation of HA in the course of the tunnel barrier formation.

Since the problem of ordering of HA films is one of the key issues in the application for spintronic devices, we have investigated kinetics of the ordering in  $\text{Co}_2\text{MnGa}$  HA film.  $\text{Co}_2\text{MnGa}$  has been shown [2] to reveal almost half-metallic behaviour. To obtain the  $\text{Co}_2\text{MnGa}$  alloy films with utmost disorder, they were vapour quenched onto the substrates cooled with liquid nitrogen. The as-deposited  $\text{Co}_2\text{MnGa}$  films were annealed at 293 (RT), 513, 598 and 728 K in high vacuum conditions. The resulting various structural states of  $\text{Co}_2\text{MnGa}$  HA films will be referred to as 1, 2, 3 and 4, respectively, to correspond to the above annealing conditions.

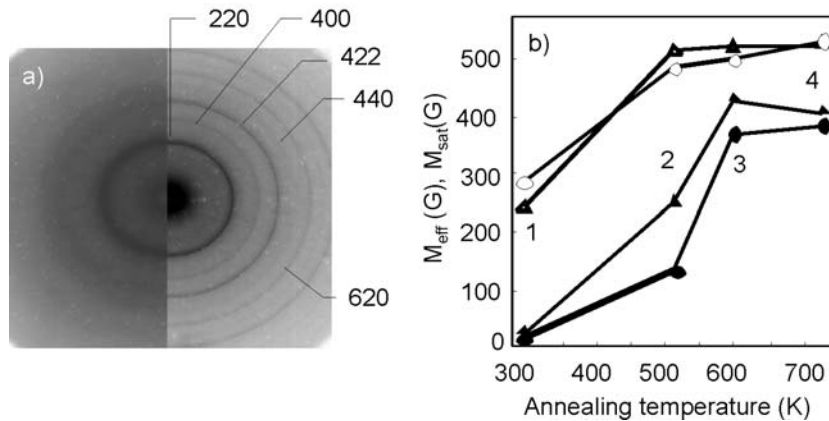


Fig. 4. TEM diffraction patterns of  $\text{Co}_2\text{MnGa}$  alloy films (a) deposited onto a substrate cooled with liquid nitrogen (left panel) and post annealed at 630 K (right panel); the saturation ( $M_S$ ) and effective ( $M_{\text{eff}}$ ) magnetization of  $\text{Co}_2\text{MnGa}$  films (b) as a function of annealing temperature.

The numbers 1–4 denote corresponding films (see text)

Figure 4a (left panel) shows transmission electron microscopy (TEM) diffraction patterns of the  $\text{Co}_2\text{MnGa}$  film deposited onto a NaCl substrate cooled with liquid nitrogen. It is clearly seen that vapour quenching deposition onto cooled substrates leads to formation of an amorphous (nanocrystalline) state. After annealing at 630 K, the amorphous film becomes crystalline with the diffraction lines characteristic of  $B2$  HA structure (Fig. 4a, right panel). A thorough X-ray diffraction characterization of the films annealed at  $T > 600$  K suggests even the presence of  $L2_1$  ordering for film 4. Generally, annealing of the vapour quenched  $\text{Co}_2\text{MnGa}$  films results in the formation of the amorphous,  $A2$ ,  $B2$  and  $L2_1$  ordering for the films 1, 2, 3 and 4, respectively.

Figure 4b shows the dependence of RT values of  $M_S$  (full symbols) and  $M_{\text{eff}}$  (open symbols) on annealing temperature corresponding to the films 1, 2, 3, and 4, respectively. The amorphous film 1 is only weakly magnetic with  $M_S \approx 25$  G. However,  $M_{\text{eff}}$  of  $\sim 200$ – $300$  G, estimated from the position of the most intensive ferromagnetic (FMR) absorption, suggests its inhomogeneous magnetic state with local effective fields  $4\pi M_{\text{eff}}$  as high as  $\sim 3000$  G. Annealing at elevated temperatures results in a substantial increase in both  $M_S$  and  $M_{\text{eff}}$  up to 400 and 500 G, respectively. Since  $M_S$  of the films 3 and 4 is practically the same, we argue that there is practically no difference in the magnetic properties of the  $\text{Co}_2\text{MnGa}$  films with  $B2$  and  $L2_1$  type of ordering. However, the saturation magnetization  $M_S$  ( $M_S \approx 450$  G,  $2.5\mu_B$  per formula unit) of our films with the highest ordering is still lower than that of the bulk ( $4\mu_B$ ) [2] and  $\text{Co}_2\text{MnGa}$  epitaxial films ( $3.5\mu_B$ ) [29]. Moreover,  $M_S$  and  $M_{\text{eff}}$  differ substantially what may be related to a high easy plane anisotropy of  $\text{Co}_2\text{MnGa}$  films due to magnetostriction [29].

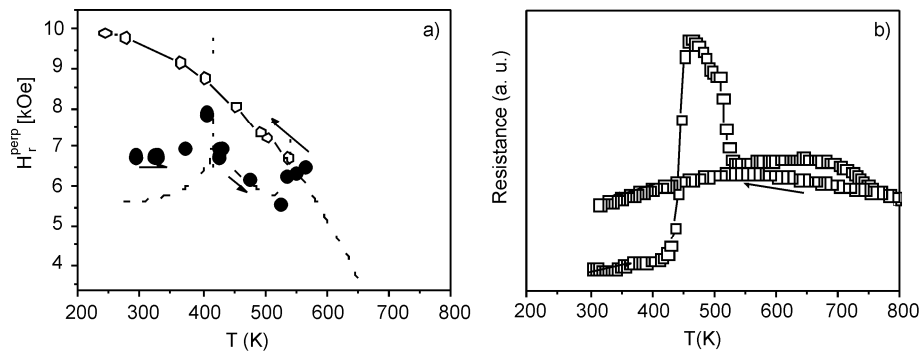


Fig. 5. Changes of FMR resonance field  $H_r^{\text{perp}}$  in the course of heating (full circles) and cooling (full diamonds) of an initially amorphous  $\text{Co}_2\text{MnGa}$  film (a); resistivity of the same  $\text{Co}_2\text{MnGa}$  film in the course of heating to  $\sim 800$  K and cooling to RT (b)

Using high-temperature FMR [30] measurements in the perpendicular configuration, we checked the temperature range in which the amorphous  $\text{Co}_2\text{MnGa}$  films order. Figure 5a shows temperature changes of the resonance field  $H_r^{\text{perp}}$  in the course of temperature cycling from RT to 570 K and back RT. In the range of ca. 420–430 K, the resonance field increases sharply, then it decreases in a way typical of a ferromagnetic

film with  $T_C$  of 600 K and eventually at  $\sim 550$  K it grows again. In the cooling cycle, the temperature changes of the resonance field  $H_r^{\text{perp}}$  are typical of a well ordered  $\text{Co}_2\text{MnGa}$  alloy with  $T_C$  of  $\sim 650$  K. These anomalies in the behaviour of  $H_r^{\text{perp}}$  vs.  $T$  strongly suggest the presence of two structural transformations in amorphous  $\text{Co}_2\text{MnGa}$  at 430 and 540 K, respectively. Comparing FMR results shown in Fig. 5a with the TEM results, we supposed that these anomalies are related to the “amorphous  $\rightarrow$  A2” and “A2  $\rightarrow$  B2” transformations, respectively. However, the electric resistivity  $\rho$  of the initially amorphous  $\text{Co}_2\text{MnGa}$  film experiences a sharp increase between 450 and 540 K and then at  $T \approx 550$  K it decreases again to a considerably higher value than that of the amorphous film, and slightly decreases at  $T > 750$  K (Fig. 5b). Our preliminary TEM studies of the structure of the films annealed between 450 K and 540 K suggest formation of a two-phase metastable structure in this temperature region. In the temperature dependence on the cooling cycle,  $\rho$  shows a semiconductor-like behaviour at  $550 > T > 800$  K with a negative coefficient of resistivity and a metallic behaviour below 600–550 K. Both a high value of the resistivity in B2 structural ordering and the change in the temperature dependence of the resistivity may result from half-metallic behaviour of the ordered  $\text{Co}_2\text{MnGa}$  films.

In summary, we have shown, that unlike amorphous  $\text{Ni}_2\text{MnZ}$  ( $Z = \text{In}, \text{Ga}, \text{Ge}$ ) films,  $\text{Co}_2\text{MnGa}$  films in the amorphous state exhibit some weak ferromagnetic behaviour. According to the FMR and resistivity results, formation of an inhomogeneous metastable structure in the temperature range of 450–550 K has been observed. The structural “A2(B2)  $\rightarrow$   $L2_1$ ” transition causes more significant increase in  $M_S$  and  $M_{\text{eff}}$  than the “amorphous state  $\rightarrow$  A2” one. However, the saturation magnetization ( $M_S \approx 450$  G,  $2.5\mu_B$  per formula unit) of our films with the highest ordering is still lower than that of the bulk ( $4\mu_B$ ) and of  $\text{Co}_2\text{MnGa}$  epitaxial films ( $3.5\mu_B$ ). Resistivity behaviour of the well ordered  $\text{Co}_2\text{MnGa}$  films suggests their half-metallic properties.

### 3. Ferromagnetic Heusler alloy films with shape memory effect

Ferromagnetic shape memory (FSM) alloys are a class of materials undergoing thermodynamically reversible martensitic transformations in a ferromagnetic state [3]. Such a structural phase transformation of a martensitic type has been reported in ternary intermetallic compounds Co–Ni–Al and Co–Ni–Ge and in iron(cobalt)-based alloys such as Fe–Pd(Pt) and Co–Ni and in Ni–Mn–Al, Co–Ni–Ga HA.

Ni–Mn–Ga HA with various stoichiometries have been the most extensively investigated FSM materials. For bulk stoichiometric  $\text{Ni}_2\text{MnGa}$ , the Curie temperature  $T_C = 376$  K and the martensitic transformation (MT) temperature is  $T_M \approx 200$  K [1]. Above  $T_M$ ,  $\text{Ni}_2\text{MnGa}$  adopts  $L2_1$  structure (Fig. 1). In the martensite phase  $\text{Ni}_2\text{MnGa}$  transforms into a twinned structure (as shown schematically in Fig. 6) composed of tetragonal phase with an enhanced anisotropy [3]. Generally, for the nonstoichiometric Ni–Mn–Ga HA there are several different martensite structures of tetragonal or

orthorhombic symmetry. Some of them are modulated with a shuffling of the (110) atomic planes with a period of five (5M) or seven (7M) atomic planes [31, 32], or unmodulated [33, 34]. The lattice constant ratios give the maximum strain which is available from the twin rearrangement. This limit is of 6% in the 5M structure [35], and of 10% in the orthorhombic 7M martensite of  $\text{Ni}_{1.95}\text{Mn}_{1.19}\text{Ga}_{0.86}$  [7].

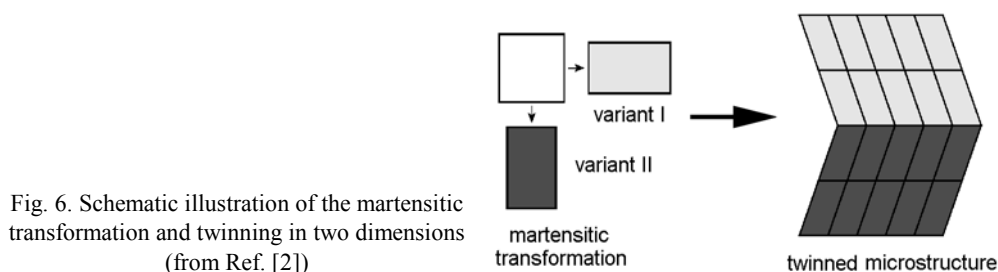


Fig. 6. Schematic illustration of the martensitic transformation and twinning in two dimensions (from Ref. [2])

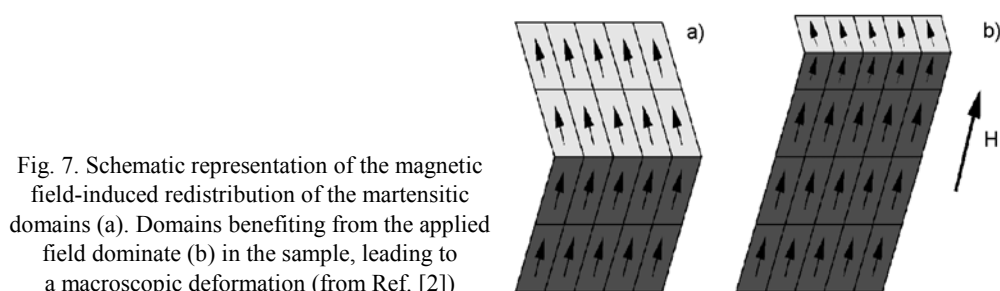


Fig. 7. Schematic representation of the magnetic field-induced redistribution of the martensitic domains (a). Domains benefiting from the applied field dominate (b) in the sample, leading to a macroscopic deformation (from Ref. [2])

As is shown in Fig. 7, magnetic fields or stress can rearrange the volume fraction of martensitic variants by the motion of twin boundaries to minimize the total energy. Such a rearrangement of the martensitic variants with magnetic field results in a large reversible strain. This change of crystallographic domain population by the application of an external magnetic field is the mechanism for the FSM effect (Fig. 7). Depending on a composition, the temperature of the phase transformation can be tuned in a wide range [4]. The large strain and ability to tune the temperature of transformation with the composition make Ni–Mn–Ga alloys a very attractive candidate for magnetic field driven actuators.

Recent efforts have focused on enabling the ferromagnetic shape memory or thermal shape memory effects on micrometer or smaller scales. Figure 8a shows a conceptual design of a microactuator [36]. A film is assumed to be deposited on the substrate in the austenite state, and is unstressed and released from a substrate. At high temperatures the film is in the austenite and is undeformed as shown in Fig. 8a in the left panel. On cooling, the film transforms to the martensite and bulges (Fig. 8a, right panel). Such tiny “machines” have been created [37] in reality (Fig. 8b). To design such “micromachines”, free-standing single crystal Ni–Mn–Ga films would be the best candidate since they allow the formation of austenite/single variant interfaces resulting in a specific tent-like deformation in the martensite phase. Recently, single

crystal  $\text{Ni}_2\text{MnGa}$  and  $\text{Ni}_2\text{Mn}_{1.2}\text{Ga}_{0.8}$  films (900 Å thick) have been grown by molecular beam epitaxy on (001) GaAs substrates with ScErAs interlayer [10]. The films were ferromagnetic with the Curie temperature of  $\sim 340$  K. It has been observed that constraint of the substrate inhibited martensitic transformation, but after removal of the substrates to release the films, it enabled a martensitic phase transformation in the free-standing single crystal films to occur. In particular, the  $\text{Ni}_2\text{Mn}_{1.2}\text{Ga}_{0.8}$  films transformed into martensite phase at RT and showed the two-way shape memory effect upon thermal cycling. The ferromagnetic shape memory effect was demonstrated in free-standing stoichiometric  $\text{Ni}_2\text{MnGa}$  bridges and cantilevers at 135 K with magnetic field applied perpendicular to the sample surface but with no quantitative measurements of the effect.

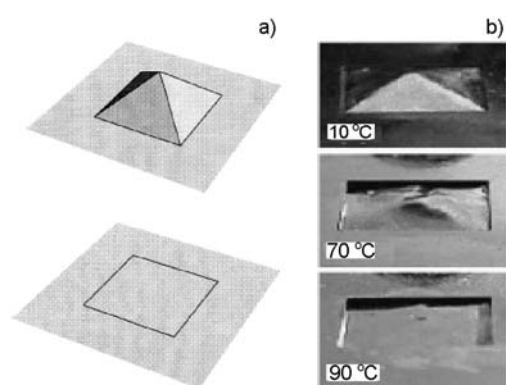


Fig. 8. A tent-like deformation of a film, which is flat in the austenite phase (a) (from Ref. [36]); realization of such a deformation in a CuAlNi foil, released on a 1 cm by 1 cm region, produced by heating and cooling the film (b) (from Ref. [37])

Wuttig et al. [38] reported phase transformations in polycrystalline sputtered 1  $\mu\text{m}$  thick Ni–Mn–Ga films deposited on Si cantilevers. They noticed that the films deposited on substrates held above 385 °C or annealed at 400 °C show an austenite/martensite transformation comparable to NiTi shape memory films.

Suzuki et al. [39] and M. Ohtsuka et al. [9] deposited 5  $\mu\text{m}$  thick Ni–Mn–Ga films by sputtering on poly(vinyl alcohol) substrates. After separating from the substrates, the films were annealed at  $\sim 1100$  K for ordering. They detected the martensitic transformation at  $\sim 250$  K and  $\sim 320$  K for the films of nominal composition  $\text{Ni}_2\text{MnGa}$  and  $\text{Ni}_{2.17}\text{MnGa}$ , respectively. The two-way shape memory effect for the constraint-aged films was confirmed as well as a small (of 0.08%) FSM effect was detected under application of the external magnetic field of 5 T [9].

Using a new technique of ultra-high vacuum magnetron sputtering from Ni, Mn and  $\text{Ni}_2\text{Ga}_3$  targets, Takeuchi et al. [12] produced thin film composition spreads onto micromachined arrays of mechanical cantilever libraries. They succeeded in detecting structural transformations and determined crystal structure with a scanning X-ray microdiffractometer, and performed a quantitative magnetization mapping of the spreads. They found that a large previously unexplored region outside the Heusler composition contains reversible martensites that are also ferromagnetic. There were also some attempts to produce Ni–Mn–Ga thin films by laser ablation [11, 40] but the

results obtained did not show any clear signs of MT. We observed some signs of martensitic transformation in the flash-evaporated Ni–Mn–Ga films on mica substrates [41].

The presence of MT in thin films is a prerequisite for any applications in MEMS. However, MT in Ni–Mn–Ga films is much less documented and the results show that the transformation is governed by microstructure [42], constraint from substrates [10] and by structural ordering [9]. Here, we show some new results concerning the influence of MT on the magnetic, electrical and thermal shape memory effect in the sputter deposited Ni–Mn–Ga films.

The films (0.5–1  $\mu\text{m}$ ) were deposited by face-to-face sputtering onto rotating glass and mica substrates held at RT. The composition of the films was determined by X-ray fluorescence and was changed in a wide range from  $\text{Ni}_{60}\text{Mn}_{20}\text{Ga}_{20}$  to  $\text{Ni}_{48}\text{Mn}_{31}\text{Ga}_{21}$  by altering the configuration of Mn and Ni pieces placed on the targets. The  $\text{Ni}_{49}\text{Mn}_{29.6}\text{Ga}_{21.4}$  (A) and  $\text{Ni}_{56.4}\text{Mn}_{21.8}\text{Ga}_{21.8}$  (B) films were chosen for further characterization since they revealed MT at RT and well above the Curie temperature of  $\sim 360$  K. The X-ray fluorescence spectroscopy confirmed a very uniform composition profiles of our sputtered samples. The films were annealed in  $10^{-4}$  Pa vacuum at 873 K for 1 h. The structural characterization of the films was carried out by XRD using  $\text{CuK}\alpha$  radiation with the sample tilted at an angle of  $2^\circ$  from the diffraction plane to suppress the reflections from mica substrates. The magnetic properties of our Ni–Mn–Ga films were investigated using FMR spectrometer operating at 9.08 GHz at temperatures from 78 K to 400 K in a magnetic field applied perpendicular and parallel to the film plane. The values of  $4\pi M_{\text{eff}}$  were determined from the resonance fields  $H^{\text{perp}}$  taken in the perpendicular configuration at various temperatures;  $\omega/\gamma = H^{\text{perp}} - 4\pi M_{\text{eff}}$ , where  $\omega = 2\pi f$  is a microwave angular frequency and  $\gamma$  is the gyromagnetic ratio corresponding to the  $g$  factor of 2 [43].

XRD patterns of our films show typically few broad peaks with (220) as the most prominent reflection (Fig. 9a) due to a high (110) texture. As we will show later, MT in the film A onsets at 310–320 K. Interestingly, the (220) peak of the film A is fairly broad of  $\sim 1^\circ$  and does not split, a typical feature of our films with MT about RT. This suggests that the (220) reflection is formed by overlapping peaks both from austenite and martensite phases. The position of the (220) peak gives the cubic lattice constant  $a = 0.581$  nm, the same as in bulk  $\text{Ni}_2\text{MnGa}$ . Film 9b with a higher MT temperature of  $\sim 420$  K reveals in XRD the split (202) and (220) peaks characteristic of the tetragonal structure with  $a = b = 0.59$ , and  $c = 0.558$  nm ( $c/a = 0.946$ ).

Figure 10a shows the temperature behaviour of magnetic properties of film 9a; the saturation magnetization  $4\pi M_{\text{S}}$ , the effective magnetization  $4\pi M_{\text{eff}}$  and the FMR linewidth  $\Delta H$ . Figure 10b shows the temperature dependence of the electric resistance  $R(T)$  of the same film. An apparent slope change in  $R(T)$  is indicative of the ferromagnetic-paramagnetic transition at the Curie temperature  $T_{\text{C}} = 365$  K while an anomalous increase of  $\sim 10\%$  in  $R(T)$  from 330 to 260 K is due to MT.

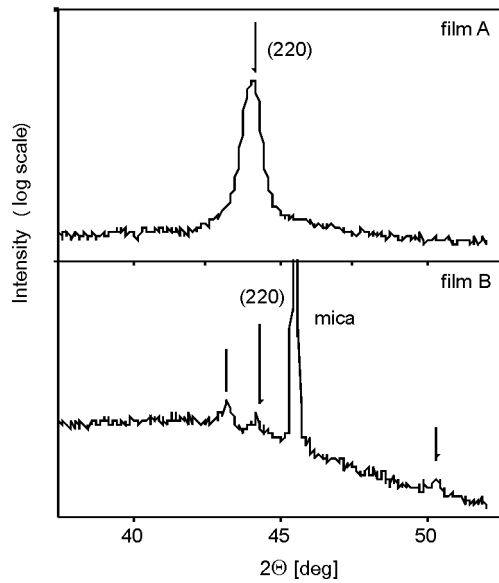


Fig. 9. XRD scans of the  $\text{Ni}_{49}\text{Mn}_{29.6}\text{Ga}_{21.4}$  (A) and  $\text{Ni}_{56.4}\text{Mn}_{21.8}\text{Ga}_{21.8}$  (B) films deposited on mica substrates. The scans were taken at RT in  $\theta$ - $2\theta$  geometry with the substrate tilted slightly from the diffraction plane in order to remove (a) or to suppress (b) the reflections from mica

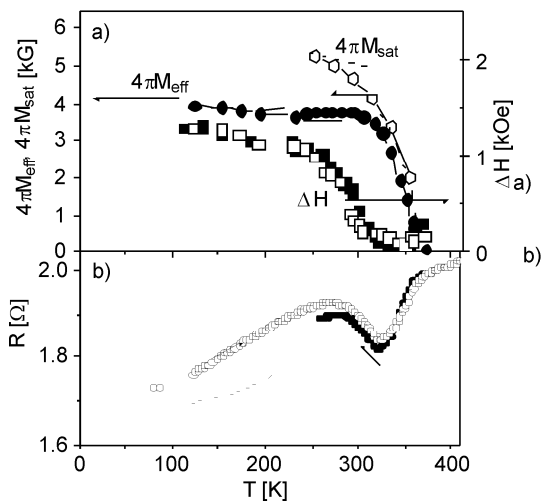


Fig. 10. Temperature dependences of the saturation magnetization  $4\pi M_{\text{sat}}$ , the effective magnetization  $4\pi M_{\text{eff}}$ , the FMR linewidth  $\Delta H$  (a) and temperature dependence of the electric resistance (b) of an  $\text{Ni}_{49}\text{Mn}_{29.6}\text{Ga}_{21.4}$  film (film A)

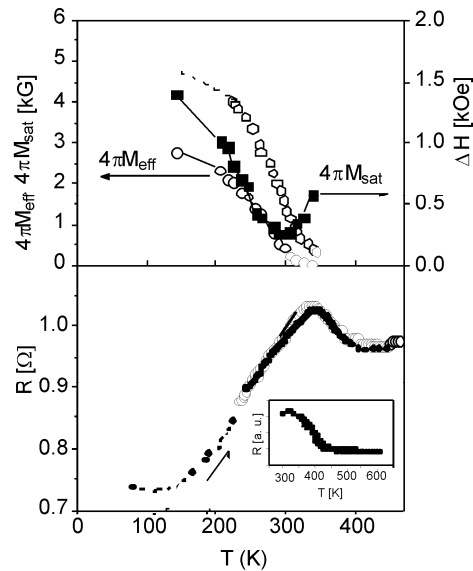


Fig. 11. Temperature dependences of the saturation magnetization  $4\pi M_{\text{s}}$ , the effective magnetization  $4\pi M_{\text{eff}}$ , the FMR linewidth  $\Delta H$  (a) and temperature dependence of the electric resistance  $R$  (b) of an  $\text{Ni}_{56.4}\text{Mn}_{21.8}\text{Ga}_{21.8}$  film (film B); inset in (b) shows  $R(T)$  of the film B measured independently at elevated temperatures

An anomalous jumplike feature in  $R(T)$  is characteristic of MT in bulk Ni–Mn–Ga alloys [4]. However, in the film A it extends from the martensitic start ( $M_s$ ) to finish ( $M_f$ ) temperatures:  $M_s = 310$  K to  $M_f = 260$  K, i.e., the temperature range is much broader than in bulk alloys [44]. Similar extended anomalies due to MT appear in the magnetic behaviour shown in Fig. 10a. While the temperature dependence of  $4\pi M_{\text{sat}}$  is quite monotonic and saturates at  $\sim 6$ – $6.5$  kG (i.e.,  $M_{\text{sat}} \approx 500$  G at 0 K), the growth in  $4\pi M_{\text{eff}}$  in the martensite phase is strongly diminished and  $4\pi M_{\text{eff}}$  exhibits a hysteretic behaviour. Simultaneously, the FMR linewidth (measured in the perpendicular configuration) strongly increases from about 100 Oe (at 330 K, i.e., in the austenite phase) to about 1.5 kOe at 100 K (in the martensite phase). Such a behaviour is typical of the martensitic transformation of relatively thick (0.5–1  $\mu\text{m}$ ) Ni–Mn–Ga films [44] in which, probably due to a constraint from the substrates (in our case mica), the transformation region is strongly extended. In much thinner Ni–Mn–Ga films the effect of MT is almost completely suppressed [41].

In Figure 11a we show the temperature dependences of  $4\pi M_{\text{eff}}$  and  $\Delta H$  in the film B with the martensitic transformation above  $T_C = 350$  K. As follows from the temperature dependence of the electrical resistance (Fig. 11b), MT extends in this film from  $M_s = 420$  K to  $M_f = 330$  K. While the magnetic characteristics ( $4\pi M_{\text{eff}}$  and  $\Delta H$ ) in the film A (with  $M_s < T_C$ ) clearly show the anomalous behaviour in the martensitic phase (Fig. 10a), in film B (with  $M_s > T_C$ ) they change monotonically. However,  $4\pi M_{\text{eff}}$  obtained from FMR attains at low temperatures the values of 3–3.5 kG, that is much lower than  $4\pi M_{\text{sat}}$  of  $\sim 6$  kG measured with VSM, and  $\Delta H$  values near  $T_C$  are substantially higher than that in the film A in the austenite phase. Such a behaviour of the magnetic properties is typical of Ni–Mn–Ga films with a columnar microstructure [41] and results from a rather complicated interplay between the shape anisotropy related to the microstructure and a substantial magnetocrystalline anisotropy in the martensite phase [3].

In the film B, we also checked the shape memory effect induced by thermal changes. For this purpose the  $\text{Ni}_{56.4}\text{Mn}_{21.8}\text{Ga}_{21.8}$  film was partially released from the mica substrate. Since an Ni–Mn–Ga film deposited by sputtering is always under severe tension, it is curled in the form of a spring after releasing from the substrate as is shown in Fig. 12a, upper panel. The radius of curvature  $r$  of the released film B was measured as a function of temperature. The radius reversibly increased on heating (Fig. 12a, bottom panel) and then decreased on cooling in a repeatable manner characteristic of two-way shape memory behaviour [9]. The resulting film strain  $\varepsilon$  versus  $T$  (defined as  $\varepsilon = d/2r$ , where  $d = 1$   $\mu\text{m}$  is the film thickness) is shown in Fig. 12b. It is seen that the shape recovery arises in the temperature range of 420–330 K in agreement with the results of the electrical resistance measurements but a substantial thermal hysteresis of  $\sim 50^\circ$  should be rather attributed to some friction between the curled “spring” windings than to the fairly narrow intrinsic hysteretic behaviour of the shape memory effect (see the inset in Fig. 11b). We estimated the magnitude of the strain change accompanied by MT as  $\Delta\varepsilon \approx 0.2\%$  resulting from the radii of 0.2 mm and

20 mm of the curled film and that after almost perfect recovery, respectively. It is interesting that the shape memory effect in the film A was much weaker.

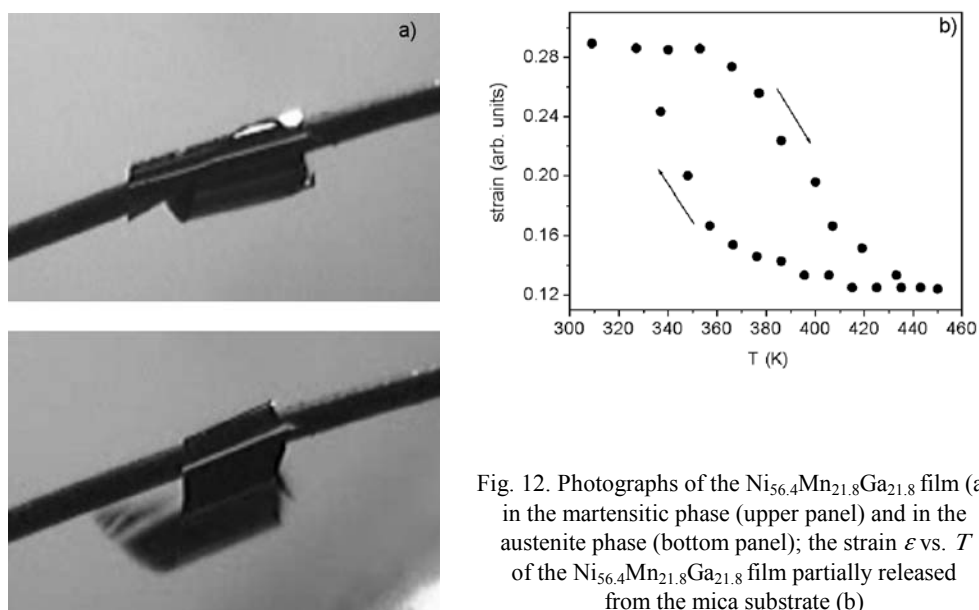


Fig. 12. Photographs of the  $\text{Ni}_{56.4}\text{Mn}_{21.8}\text{Ga}_{21.8}$  film (a) in the martensitic phase (upper panel) and in the austenite phase (bottom panel); the strain  $\epsilon$  vs.  $T$  of the  $\text{Ni}_{56.4}\text{Mn}_{21.8}\text{Ga}_{21.8}$  film partially released from the mica substrate (b)

In summary, we have observed the influence of the martensitic transformation on the magnetic and electrical properties in Ni–Mn–Ga films with MT below and above  $T_C$ . An anomalous behaviour of the magnetic properties of Ni–Mn–Ga films in the martensite phase has been compared with the electrical resistance vs.  $T$  characteristics. The temperature range of MT in our films has been found to be much broader in comparison to that in the bulk Ni–Mn–Ga alloys. The two-way shape memory effect has been confirmed in our films.

#### 4. Conclusions

We reviewed the current status of the technology of the Heusler alloy films with a special emphasis on possible applications of highly sensitive TMR sensors in spintronics as well as in micro-electromechanical systems.

#### Acknowledgements

Financial support of the Polish Committee for Scientific Research, Grant No. 4 T08C 045 25 is gratefully acknowledged.

## References

- [1] WEBSTER P.J., *Contemp. Phys.*, 10 (1969), 559.
- [2] GALANAKIS I., DEDERICHS P.H., [in:] *Half-metallic Alloys. Fundamentals and Applications*, I. Galanakis, P. H. Dederichs (Eds.), Springer, Berlin, 2005, pp. 1–34.
- [3] ENKOVAARA J., AYUELA A., ZAYAK A.T., ENTEL P., NORDSTROM M., DUBE L., JAKALEN J., IMPOLA J., NIEMINEN R.M., *Mater. Sci. Eng. A*, 376 (2004), 52.
- [4] VASIL'EV A.N., BUCHEL'NIKOV V.D., TAKAGI T., KHOVAILO V.V., ESTRIN E.I., *Phys. Usp.*, 46 (2003), 559; <http://arxiv.org/abs/cond-mat/0311433>.
- [5] DE GROOT R.A., MUELLER F.M., VAN ENGEN P.G., BUSCHOW K.H.J., *Phys. Rev. Lett.*, 50 (1983), 2024.
- [6] ISHIDA S., AKAZAWA S., FUJII S., KASHIWAGI S., ASANO S., *J. Phys. Soc. Jpn.*, 64 (1995), 2152.
- [7] SOZINOV A., LIKHACHEV A.A., LANSKA N., ULLAKO K., *Appl. Phys. Lett.*, 80 (2002), 1746.
- [8] KOYAMA K., WATANABE K., KANOMATA T., KAINUMA R., OIKAWA K., ISHIDA K., *Appl. Phys. Lett.*, 88 (2006), 132505.
- [9] OHTSUKA M., SANDA M., MATSUMOTO M., ITAGAKI K., *Mater. Sci. Eng. A*, 378 (2004), 378.
- [10] DONG J.W., XIE J.Q., LU J., ADELMANN C., PALMSTROM C.J., SUI J., PAN Q., SHIELD T.W., JAMES R.R.D., MCKERNAN S., *J. Appl. Phys.*, 95 (2004), 2593.
- [11] CASTANO F.J., NELSON-CHEESEMAN B., O'HANDLEY R.C., ROSS C.A., REDONDO C., CASTANO F., *J. Appl. Phys.*, 93 (2003), 8492.
- [12] TAKEUCHI I., FAMODU O.O., READ J.C., ARONOVA M.A., CHANG K.-S., CRACIUNESCU C., LOFLAND S.E., WUTTIG M., WELLSTOOD F.C., KNAUSS L., OROZCO A., *Nature Mat.*, 2 (2003), 180.
- [13] WOLF S.A., AWSCHALOM D.D., BURHMAN R.A., DAUGHTON J.M., VON MOLNAR S., ROUKES M.L., CHITCHEKLANOVA A.Y., TREGER D.M., *Science*, 294 (2001), 1488.
- [14] BLOCK T., FELSER C., JAKOB G., ENSLING J., MUHLING B., GUTLICH P., CAVA R.J., *Sol. St. Chem.* 176 (2003), 646.
- [15] FELSER C., ELMERS H.-J., FECHER G.H., [in:] *Half-Metallic Alloys. Fundamentals and Applications*, I. Galanakis, P. H. Dederichs (Eds.), Springer-Verlag, Berlin, 2005, pp. 113-149.
- [16] GALANAKIS I., *J. Phys. Cond. Matter*, 16 (2004), 3089.
- [17] UMETSU T.Y., KOBAYASHI K., FUJITA A., OIKAWA K., KAINUMA R., ISHIDA K., ENDO N., FUKAMICHI K., SAKUMA A., *Phys. Rev. B*, 72 (2005), 214412.
- [18] INOMATA K., OKAMURA S., GOTO R., YEZUKA N., *Jpn. J. Appl. Phys.* 42 (2003), L419.
- [19] RAPHAEL M., RAVEL B., WILLARD M., CHENG S., DAS B., HARRIS R., BUSSMANN K., CLASSEN J., HARRIS U., *Appl. Phys. Lett.*, 81 (2002), 2812.
- [20] *Polarized Electrons in Surface Physics*, R. Feder (Ed.), World Scientific, Singapore, 1985.
- [21] TEDROW P.M., MASEVEY R., *J. Appl. Phys.*, 76 (1994), 6101.
- [22] SOULEN J., BYERS J.M., OSOFSKY M.S., NADGORNÝ B., AMBROSE T., CHENG S.F., BROUSSARD P.R., TANAKA C.T., NOWAK J., MOODERA J.S., BARRY A., COEY J.M.D., *Science*, 282 (1998), 85.
- [23] CLIFFORD E., VENKANESAN M., GUNNING R., COEY J.M.D., *Sol. State Comm.*, 131 (2004), 61.
- [24] HÜTTEN A., KAMMERER S., SCHMALHORST J., REISS G., [in:] *Half-metallic Alloys. Fundamentals and Applications*, I. Galanakis, P. H. Dederichs (Eds.), Springer-Verlag, Berlin, 2005, pp. 241–264.
- [25] INOMATA K., TEZUKA N., OKAMURA S., KUREBAYASHI H., HIROKATA A., *J. Appl. Phys.*, 95 (2004), 7234.
- [26] SAKUBARA Y., NAKATA J., OOGANE M., KATO H., SAKUMA A., MIYAZAKI T., KUBOTA H., *Appl. Phys. Lett.*, 88 (2006), 022503.
- [27] KUBOTA H., NAKATA J., OOGANE M., SUKUMA A., MIYAZAKI T., *Jpn. J. Appl. Phys., Part 2*, 43 (2004), L984.
- [28] SCHMALHORST J., KAMMERER S., SACHER M., REISS G., HUTTEN A., SCHOLL A., *Phys. Rev. B*, 70 (2004), 024426.
- [29] PECHAN M.J., YU C., CARR D., PALMSTRÖM C.J., *J. Magn. Magn. Mater.*, 286 (2005), 340.

- [30] KUDRYAVTSEV Y.V., OKSENEKO V.A., KULAGIN V.A., DUBOWIK J., LEE Y.P., *J. Magn. Magn. Mater.*, 310 (2007), 2271.
- [31] WEBSTER P.J., ZIEBECK K.R.A., TOWN S.L., PEAK M.S., *Philos. Mag. B*, 49 (1984), 295.
- [32] MARTYNOV V.V., KOKORIN V.V., *J. Phys.*, III, 2 (1992), 739.
- [33] WANG W.H., WU G.H., CHEN J.L., GAO S.X., ZHAN W., WEN G.H., CHAN X.X., *Appl. Phys. Lett.*, 79 (2001), 1148.
- [34] CHERNENKO V.A., SEGUI C., CESARI E., PONS J., KOKORIN V.V., *Phys. Rev. B*, 57 (1998), 2659.
- [35] HECZKO O., SOZINOV A., ULLAKKO K., *IEEE Trans. Magn.*, 36 (2000), 541 3266.
- [36] BHATTACHARYA K., JAMES R.D., *J. Mech. Phys. Solids*, 47 (1999), 531.
- [37] BHACHATTARYA K., JAMES R.D., *Science*, 307 (2005), 53.
- [38] WUTTIG M., CRACIUNESCU C., LI J., *Mater. Trans. JIM*, 41 (2000), 933.
- [39] SUZUKI M., OHTSUKA M., SUZUKI T., MATSUMOTO M., MIKI H., *Mat Trans. JIM*, 40 (1999), 1174.
- [40] CHUNG C.Y., CHERNENKO V.A., KHOVAILO V.V., PONS J., CESARI E., TAKAGI T., *Mater. Sci. Engn. A*, 378 (2004), 444.
- [41] DUBOWIK J., KUDRYAVTSEV V.V., LEE Y.P., *J. Appl. Phys.*, 95 (2004), 2912.
- [42] DUBOWIK J., GOŚCIAŃSKA I., KUDRYAVTSEV Y.V., LEE Y.P., SOVAK P., KONC M., *phys. stat. sol. C*, 3 (2006), 143.
- [43] PATIL S., TANG D., LOFLAND S.E., BHAGAT S.M., TAKEUCHI I., FAMADU O., READ J.C., CHANG K.-S., CRACIUNESCU C., WUTTIG M., *Appl. Phys. Lett.*, 81 (2002), 1279.
- [44] KHOVAILO V.V., TAKAGI T., BOZHKO A.D., MATSUMOTO M., TANI J., SHAVROV V.G., *J. Phys. Cond. Matter*, 13 (2001), 9655.

*Received 7 May 2006*  
*Revised 1 September 2006*